ACTA ASTRONOMICA
Vol. **58** (2008) pp. 329–343

The Optical Gravitational Lensing Experiment. OGLE-III Photometric Maps of the Small Magellanic Cloud*

A. Udalski[1], I. Soszyński[1], M.K. Szymański[1], M. Kubiak[1], G. Pietrzyński[1,2], Ł. Wyrzykowski[3], O. Szewczyk[2], K. Ulaczyk[1] and R. Poleski[1]

[1] Warsaw University Observatory, Al. Ujazdowskie 4, 00-478 Warszawa, Poland
e-mail: (udalski,soszynsk,msz,mk,pietrzyn,kulaczyk,rpoleski)@astrouw.edu.pl
[2] Universidad de Concepción, Departamento de Fisica, Casilla 160–C, Concepción, Chile
e-mail: szewczyk@astro-udec.cl
[3] Institute of Astronomy, University of Cambridge, Madingley Road, Cambridge CB3 0HA, UK
e-mail: wyrzykow@ast.cam.ac.uk

Received December 27, 2008

ABSTRACT

We present OGLE-III Photometric Maps of the Small Magellanic Cloud. They contain precise, calibrated *VI* photometry of about 6.2 million stars from 41 OGLE-III fields in the SMC observed regularly in the years 2001–2008 and covering about 14 square degrees in the sky. Also precise astrometry of these objects is provided. One of the fields, SMC140, is centered on the 47 Tucanae Galactic globular cluster providing unique data on this object.

We discuss quality of the data and present a few color–magnitude diagrams of the observed fields.

All photometric data are available to the astronomical community from the OGLE Internet archive.

Key words: *Magellanic Clouds – Surveys – Catalogs – Techniques: photometric*

1. Introduction

One of the very important results of the second phase of the Optical Gravitational Lensing Experiment (OGLE-II) – long term, large scale photometric survey – was the publication of the OGLE Photometric Maps of Dense Stellar Regions observed regularly in the course of the project. The maps contain calibrated *BVI* or *VI* photometry and precise astrometry of millions of stars from astrophysically so

*Based on observations obtained with the 1.3 m Warsaw telescope at the Las Campanas Observatory of the Carnegie Institution of Washington.

important objects like the Large and Small Magellanic Clouds and Galactic Center (Udalski *et al.* 1998, 2000, 2002).

OGLE maps are a very important source of astrophysical information and were widely used by astronomers to many projects (*e.g.*, Evans *et al.* 2005, Coe *et al.* 2005, Chiosi and Vallenari 2007, Haberl, Eger and Pietsch 2008). The maps constitute also a huge set of secondary photometric standards and can be used for calibrating photometry.

The OGLE-II maps cover mostly the central parts of the Magellanic Clouds and about 10 square degrees of the Galactic bulge. Large upgrade of the OGLE project to OGLE-III phase in 2001 enabled regular coverage of much larger area in the sky. After several years of regular monitoring of OGLE-III targets the collected images were finally reprocessed to derive the final photometry (Udalski *et al.* 2008a). This enabled construction of new version of the maps based on OGLE-III observations. Recently the first part of the new OGLE-III map set – the maps of the Large Magellanic Cloud – has been released (Udalski *et al.* 2008b).

This paper is the next of this series. We present here new OGLE-III photometric maps of the Small Magellanic Cloud. The new maps constitute a significant extension to the OGLE-II maps of the SMC as they cover much larger area and contain many more objects. Additionally they also include the region of the very important Galactic globular cluster – 47 Tuc.

The maps are available to the astrophysical community from the OGLE Internet archive.

2. Observational Data

Observational data presented in this paper were collected during the OGLE-III phase between June 2001 and January 2008. 1.3-m Warsaw Telescope at Las Campanas Observatory, Chile, operated by the Carnegie Institution of Washington, equipped with the eight chip mosaic camera (Udalski 2003) was used. One image covers approximately 35×35 arcmins on the sky with the scale of 0.26 arcsec/pixel.

Observations were carried out in *V*- and *I*-band filters closely resembling the standard bands. One should be however aware, that the OGLE glass *I*-band filter approximates well the standard one for $V-I<3$ mag colors. For very red objects the transformation to the standard band is less precise. The vast majority of observations were obtained through the *I*-band filter. Typically several hundred images for each field were collected in this band and about 40–50 in the *V*-band. The exposure time was 180 and 240 seconds for the *I*- and *V*-band, respectively.

To obtain precise photometry in the dense regions of the SMC, observations were conducted only in good seeing (less than $1\farcs8$) and transparency conditions. The median seeing of the *I*-band images of the SMC collected during OGLE-III is equal to $1\farcs2$.

T a b l e 1

OGLE-III Fields in the SMC

Field	RA (2000)	DEC (2000)	$N_{\rm Stars}$
SMC100	$0^{\rm h}50^{\rm m}06\overset{\rm s}{.}4$	$-73^\circ08'19''$	512714
SMC101	$0^{\rm h}50^{\rm m}04\overset{\rm s}{.}0$	$-72^\circ32'57''$	342621
SMC102	$0^{\rm h}50^{\rm m}09\overset{\rm s}{.}0$	$-71^\circ57'09''$	121100
SMC103	$0^{\rm h}50^{\rm m}08\overset{\rm s}{.}6$	$-73^\circ43'44''$	274952
SMC104	$0^{\rm h}50^{\rm m}06\overset{\rm s}{.}7$	$-74^\circ19'21''$	128812
SMC105	$0^{\rm h}57^{\rm m}50\overset{\rm s}{.}8$	$-72^\circ44'37''$	365672
SMC106	$0^{\rm h}58^{\rm m}06\overset{\rm s}{.}7$	$-73^\circ20'21''$	362026
SMC107	$0^{\rm h}58^{\rm m}23\overset{\rm s}{.}0$	$-73^\circ55'50''$	142474
SMC108	$0^{\rm h}57^{\rm m}31\overset{\rm s}{.}5$	$-72^\circ09'29''$	413846
SMC109	$0^{\rm h}57^{\rm m}18\overset{\rm s}{.}8$	$-71^\circ33'56''$	132507
SMC110	$1^{\rm h}05^{\rm m}40\overset{\rm s}{.}0$	$-72^\circ44'35''$	234190
SMC111	$1^{\rm h}06^{\rm m}10\overset{\rm s}{.}2$	$-73^\circ20'12''$	181265
SMC112	$1^{\rm h}06^{\rm m}37\overset{\rm s}{.}3$	$-73^\circ55'58''$	112770
SMC113	$1^{\rm h}05^{\rm m}02\overset{\rm s}{.}8$	$-72^\circ09'32''$	281492
SMC114	$1^{\rm h}04^{\rm m}31\overset{\rm s}{.}5$	$-71^\circ34'06''$	156581
SMC115	$1^{\rm h}13^{\rm m}22\overset{\rm s}{.}4$	$-72^\circ44'27''$	110029
SMC116	$1^{\rm h}13^{\rm m}57\overset{\rm s}{.}6$	$-73^\circ20'36''$	117909
SMC117	$1^{\rm h}15^{\rm m}03\overset{\rm s}{.}4$	$-73^\circ55'34''$	47030
SMC118	$1^{\rm h}12^{\rm m}38\overset{\rm s}{.}7$	$-72^\circ08'56''$	91419
SMC119	$1^{\rm h}11^{\rm m}47\overset{\rm s}{.}8$	$-71^\circ34'05''$	102201
SMC120	$1^{\rm h}20^{\rm m}58\overset{\rm s}{.}8$	$-72^\circ45'10''$	59056
SMC121	$1^{\rm h}22^{\rm m}04\overset{\rm s}{.}2$	$-73^\circ20'24''$	31525
SMC122	$1^{\rm h}23^{\rm m}15\overset{\rm s}{.}8$	$-73^\circ55'54''$	21627
SMC123	$1^{\rm h}20^{\rm m}05\overset{\rm s}{.}9$	$-72^\circ09'17''$	34723
SMC124	$1^{\rm h}19^{\rm m}03\overset{\rm s}{.}5$	$-71^\circ34'06''$	43827
SMC125	$0^{\rm h}42^{\rm m}05\overset{\rm s}{.}2$	$-73^\circ19'43''$	384551
SMC126	$0^{\rm h}42^{\rm m}25\overset{\rm s}{.}5$	$-72^\circ43'46''$	207374
SMC127	$0^{\rm h}42^{\rm m}58\overset{\rm s}{.}5$	$-71^\circ08'45''$	21564
SMC128	$0^{\rm h}41^{\rm m}48\overset{\rm s}{.}1$	$-73^\circ55'17''$	190156
SMC129	$0^{\rm h}41^{\rm m}35\overset{\rm s}{.}4$	$-74^\circ30'26''$	56668
SMC130	$0^{\rm h}34^{\rm m}05\overset{\rm s}{.}6$	$-73^\circ19'15''$	125840
SMC131	$0^{\rm h}34^{\rm m}33\overset{\rm s}{.}6$	$-72^\circ43'47''$	71873
SMC132	$0^{\rm h}35^{\rm m}49\overset{\rm s}{.}4$	$-71^\circ08'24''$	18600
SMC133	$0^{\rm h}33^{\rm m}36\overset{\rm s}{.}8$	$-73^\circ55'03''$	101530
SMC134	$0^{\rm h}32^{\rm m}52\overset{\rm s}{.}3$	$-74^\circ30'24''$	42505
SMC135	$0^{\rm h}26^{\rm m}02\overset{\rm s}{.}8$	$-73^\circ19'22''$	54487
SMC136	$0^{\rm h}26^{\rm m}48\overset{\rm s}{.}0$	$-72^\circ43'52''$	41378
SMC137	$0^{\rm h}28^{\rm m}41\overset{\rm s}{.}8$	$-71^\circ08'22''$	15786
SMC138	$0^{\rm h}25^{\rm m}21\overset{\rm s}{.}4$	$-73^\circ55'19''$	77662
SMC139	$0^{\rm h}24^{\rm m}16\overset{\rm s}{.}3$	$-74^\circ30'25''$	33851
SMC140	$0^{\rm h}24^{\rm m}08\overset{\rm s}{.}9$	$-72^\circ04'54''$	343389

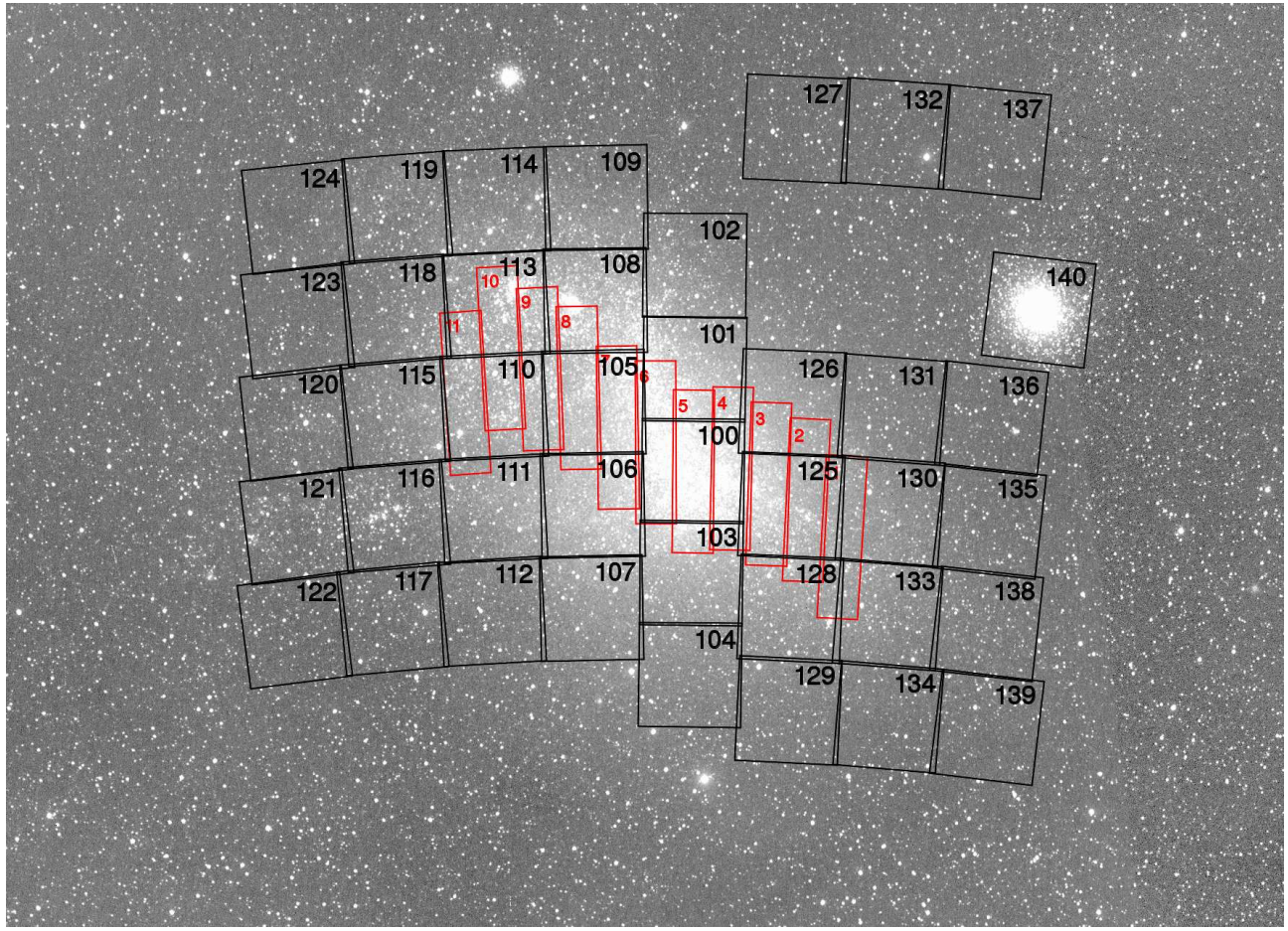

Fig. 1. OGLE-III fields in the SMC (black squares: 100–140) overplotted on the image obtained by the ASAS all sky survey. Gray strips (1–11) mark OGLE-II fields.

Table 1 lists all the SMC fields observed during OGLE-III phase as well as the equatorial coordinates of their centers and number of stars detected in the *I*-band. Fig. 1 presents an image of the SMC folded from images taken by the ASAS survey program (Pojmański 1997) with contours of the OGLE-III fields. The area of the sky covered by OGLE-III observations reaches 14 square degrees.

3. Photometric Maps of the SMC

Detailed description of the construction of the OGLE-III maps was presented by Udalski *et al.* (2008b). The procedure for the SMC maps was identical as in the case of the LMC. We only recall here that the maps contain the mean photometry of all detected stellar objects. The mean photometry was obtained for all objects with minimum 4 and 6 observations in the *V*- and *I*-band, respectively by averaging all observations after removing 5σ deviating points.

Table 2 lists as an example the first 25 entries from the map of the SMC100.1 subfield. The columns contain: (1) ID number; (2,3) equatorial coordinates J2000.0; (4,5) X,Y pixel coordinates in the *I*-band reference image; (6,7,8) photometry: V, $V-I$, I; (9,10,11) number of points for average magnitude, number of 5σ removed points, σ of magnitude for *V*-band; (12,13,14) same as (9,10,11) for the *I*-band. 9.999 or 99.999 markers mean "no data". -1 in column (9) indicates multiple *V*-band cross-identification (the average magnitude is the mean of the merged datasets).

The full set of the OGLE-III Photometric Maps of the SMC is available from the OGLE Internet archive (see Section 5).

4. Discussion

The new OGLE-III Photometric Maps of the SMC contain data for about 6.2 million stars located in 41 OGLE-III fields. The maps are significant extension to the OGLE-II maps of this galaxy (Udalski *et al.* 1998) that covered mostly the central bar. Therefore they are much better tool for studying properties of the SMC.

Typical accuracy of the OGLE-III Photometric Maps is presented in Figs. 2 and 3 where standard deviation of magnitudes as a function of magnitude in the *V*- and *I*-band is plotted. The plots are shown for the most dense central subfield SMC100.2 and empty subfield SMC138.2 located at the outskirts of this galaxy.

Completeness of the photometry can be assessed from the histograms presented in Figs. 4 and 5 for the same two subfields. It reaches $I \approx 21$ mag and $V \approx 21.5$ mag and, as expected, the photometry is deeper and more complete for less crowded fields.

Table 2

OGLE-III Photometric Map of the SMC100.2 subfield.

ID	RA (2000)	DEC (2000)	X	Y	V	$V-I$	I	N_V	$N_V^{\rm bad}$	σ_V	N_I	$N_I^{\rm bad}$	σ_I
1	$0^{\rm h}50^{\rm m}06\overset{\rm s}{.}29$	$-73°16'31\overset{''}{.}4$	250.36	18.29	13.693	−0.095	13.788	15	0	0.012	432	0	0.012
2	$0^{\rm h}50^{\rm m}08\overset{\rm s}{.}58$	$-73°15'53\overset{''}{.}1$	397.52	56.70	13.795	0.017	13.778	38	0	0.011	613	0	0.010
3	$0^{\rm h}50^{\rm m}09\overset{\rm s}{.}23$	$-73°15'15\overset{''}{.}3$	542.31	67.96	15.444	1.170	14.274	42	0	0.007	620	0	0.007
4	$0^{\rm h}50^{\rm m}13\overset{\rm s}{.}06$	$-73°17'10\overset{''}{.}2$	101.28	130.12	13.707	0.791	12.916	42	0	0.006	629	3	0.013
5	$0^{\rm h}50^{\rm m}23\overset{\rm s}{.}93$	$-73°13'20\overset{''}{.}6$	981.38	313.77	15.192	1.692	13.500	43	0	0.014	632	0	0.010
6	$0^{\rm h}50^{\rm m}29\overset{\rm s}{.}46$	$-73°16'39\overset{''}{.}7$	217.32	402.07	16.467	2.289	14.178	43	0	0.121	632	0	0.076
7	$0^{\rm h}50^{\rm m}34\overset{\rm s}{.}15$	$-73°13'54\overset{''}{.}2$	851.53	482.90	15.636	2.378	13.258	43	0	0.241	632	0	0.072
8	$0^{\rm h}50^{\rm m}34\overset{\rm s}{.}42$	$-73°13'00\overset{''}{.}9$	1056.00	488.33	14.566	9.999	99.999	43	0	0.010	0	0	9.999
9	$0^{\rm h}50^{\rm m}34\overset{\rm s}{.}61$	$-73°15'52\overset{''}{.}6$	397.47	488.27	15.038	1.046	13.992	43	0	0.005	632	0	0.007
10	$0^{\rm h}50^{\rm m}37\overset{\rm s}{.}20$	$-73°17'24\overset{''}{.}0$	46.56	529.47	13.757	−0.081	13.837	37	0	0.008	567	0	0.008
11	$0^{\rm h}50^{\rm m}36\overset{\rm s}{.}96$	$-73°13'06\overset{''}{.}3$	1035.11	530.49	15.252	1.345	13.906	43	0	0.007	632	0	0.007
12	$0^{\rm h}50^{\rm m}38\overset{\rm s}{.}03$	$-73°16'14\overset{''}{.}7$	312.41	544.55	15.536	1.539	13.997	43	0	0.011	632	0	0.008
13	$0^{\rm h}50^{\rm m}41\overset{\rm s}{.}90$	$-73°16'50\overset{''}{.}1$	176.32	608.02	14.996	1.557	13.439	43	0	0.015	632	0	0.010
14	$0^{\rm h}50^{\rm m}43\overset{\rm s}{.}63$	$-73°16'32\overset{''}{.}0$	245.73	636.94	14.979	1.174	13.804	43	0	0.006	632	0	0.006
15	$0^{\rm h}50^{\rm m}43\overset{\rm s}{.}44$	$-73°12'55\overset{''}{.}2$	1077.03	638.38	15.158	2.134	13.023	43	0	0.069	632	0	0.031
16	$0^{\rm h}50^{\rm m}46\overset{\rm s}{.}40$	$-73°13'15\overset{''}{.}4$	999.46	687.22	14.784	1.556	13.228	43	0	0.007	631	1	0.009
17	$0^{\rm h}50^{\rm m}53\overset{\rm s}{.}29$	$-73°16'51\overset{''}{.}4$	170.32	796.58	15.490	1.340	14.150	43	0	0.006	632	0	0.006
18	$0^{\rm h}50^{\rm m}54\overset{\rm s}{.}97$	$-73°17'04\overset{''}{.}0$	121.81	824.01	13.975	9.999	99.999	43	0	0.004	0	0	9.999
19	$0^{\rm h}50^{\rm m}55\overset{\rm s}{.}61$	$-73°12'54\overset{''}{.}9$	1076.78	840.67	14.259	0.553	13.706	43	0	0.009	631	1	0.007
20	$0^{\rm h}50^{\rm m}56\overset{\rm s}{.}57$	$-73°12'55\overset{''}{.}5$	1074.43	856.59	14.800	0.668	14.132	43	0	0.008	632	0	0.007
21	$0^{\rm h}50^{\rm m}57\overset{\rm s}{.}41$	$-73°17'33\overset{''}{.}4$	8.61	863.70	16.565	2.900	13.665	18	0	0.342	361	0	0.259
22	$0^{\rm h}50^{\rm m}58\overset{\rm s}{.}01$	$-73°17'08\overset{''}{.}6$	103.76	874.24	14.471	1.576	12.894	42	0	0.007	629	3	0.012
23	$0^{\rm h}51^{\rm m}01\overset{\rm s}{.}95$	$-73°16'06\overset{''}{.}9$	340.06	941.04	14.394	9.999	99.999	43	0	0.011	0	0	9.999
24	$0^{\rm h}50^{\rm m}05\overset{\rm s}{.}91$	$-73°14'06\overset{''}{.}5$	806.60	13.74	16.592	1.483	15.109	13	0	0.016	404	0	0.013
25	$0^{\rm h}50^{\rm m}06\overset{\rm s}{.}38$	$-73°13'22\overset{''}{.}3$	976.00	22.13	16.515	1.331	15.184	18	0	0.010	460	0	0.012

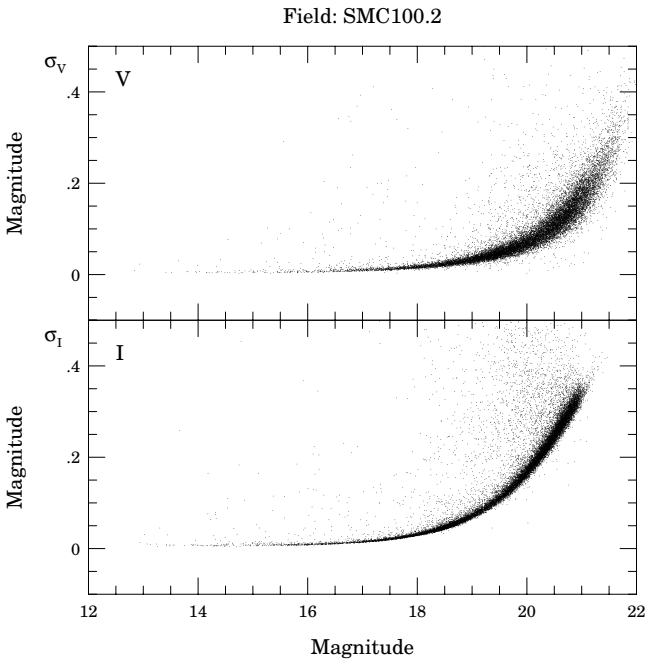

Fig. 2. Standard deviation of magnitudes as a function of magnitude for the central bar subfield SMC100.2.

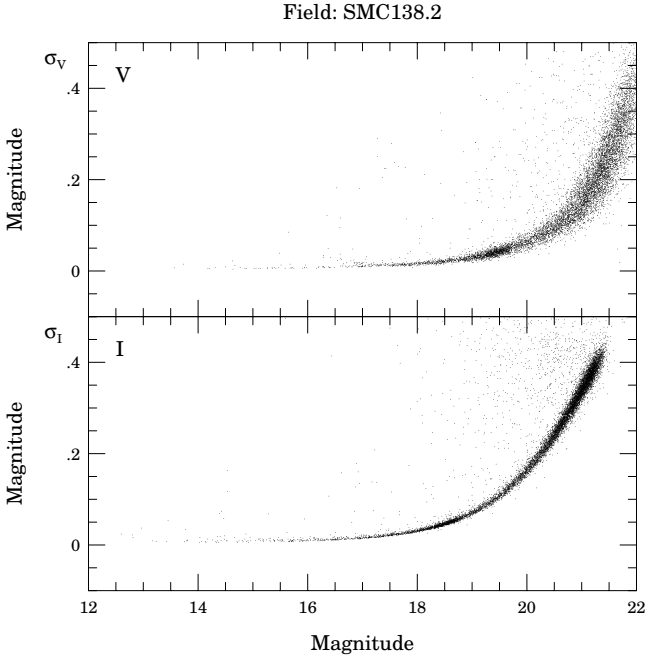

Fig. 3. Same as in Fig. 2 for the subfield SMC138.2 located in the outskirts of the SMC.

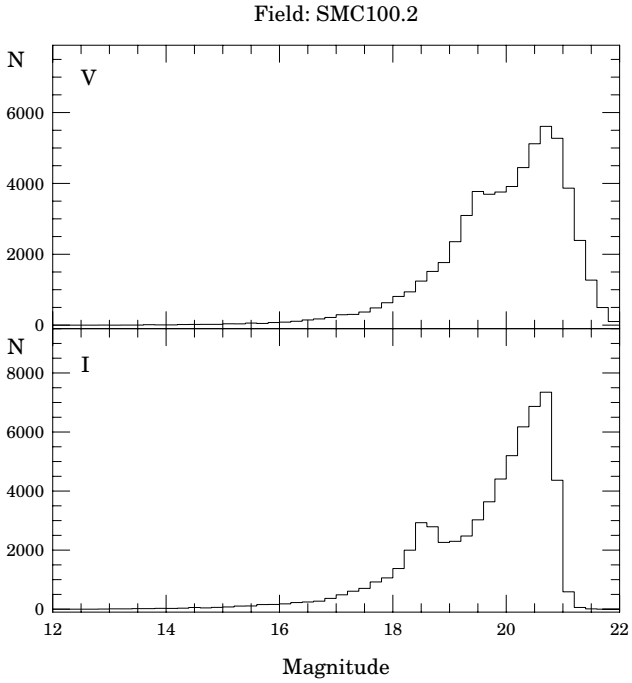

Fig. 4. Histogram of magnitudes for the central bar subfield SMC100.2.

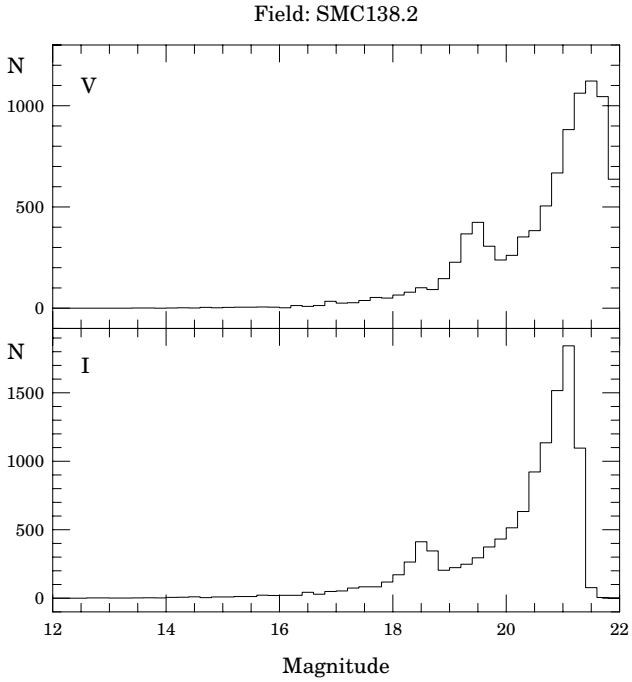

Fig. 5. Same as in Fig. 5 for the outer subfield SMC138.2.

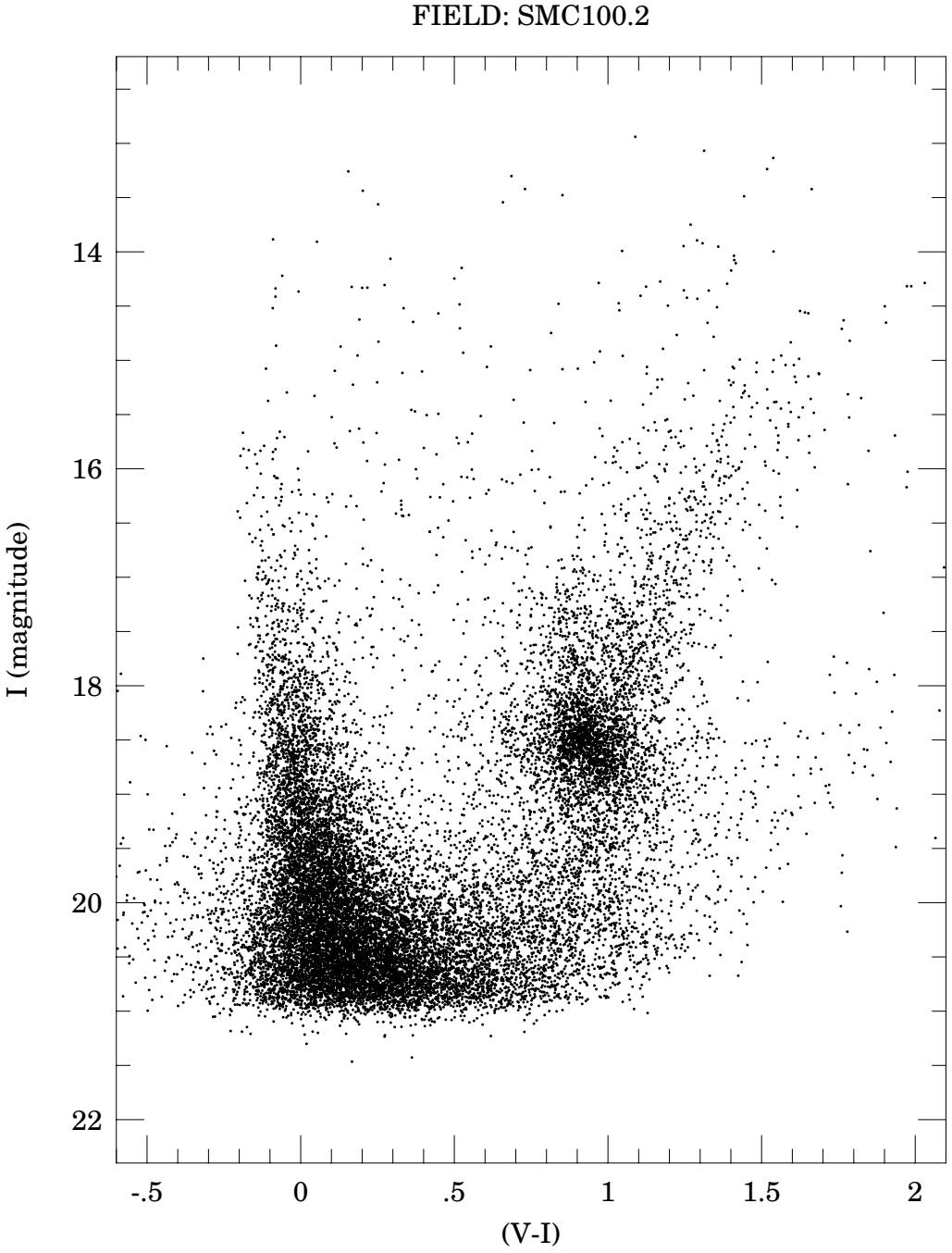

Fig. 6. Color–magnitude diagram of the central bar subfield SMC100.2. Only 30% of stars are plotted for clarity.

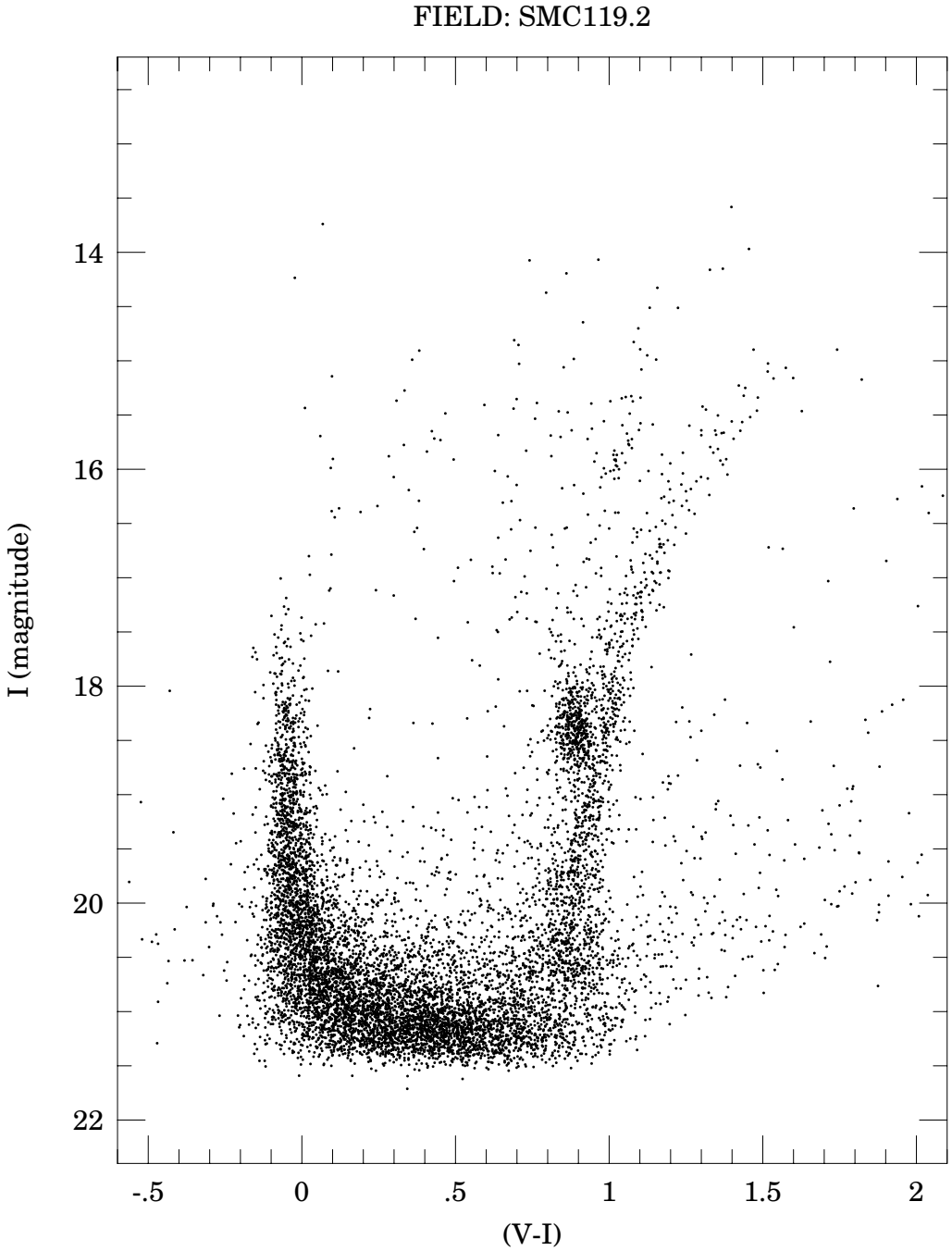

Fig. 7. Color–magnitude diagram of the eastern wing subfield SMC119.2.

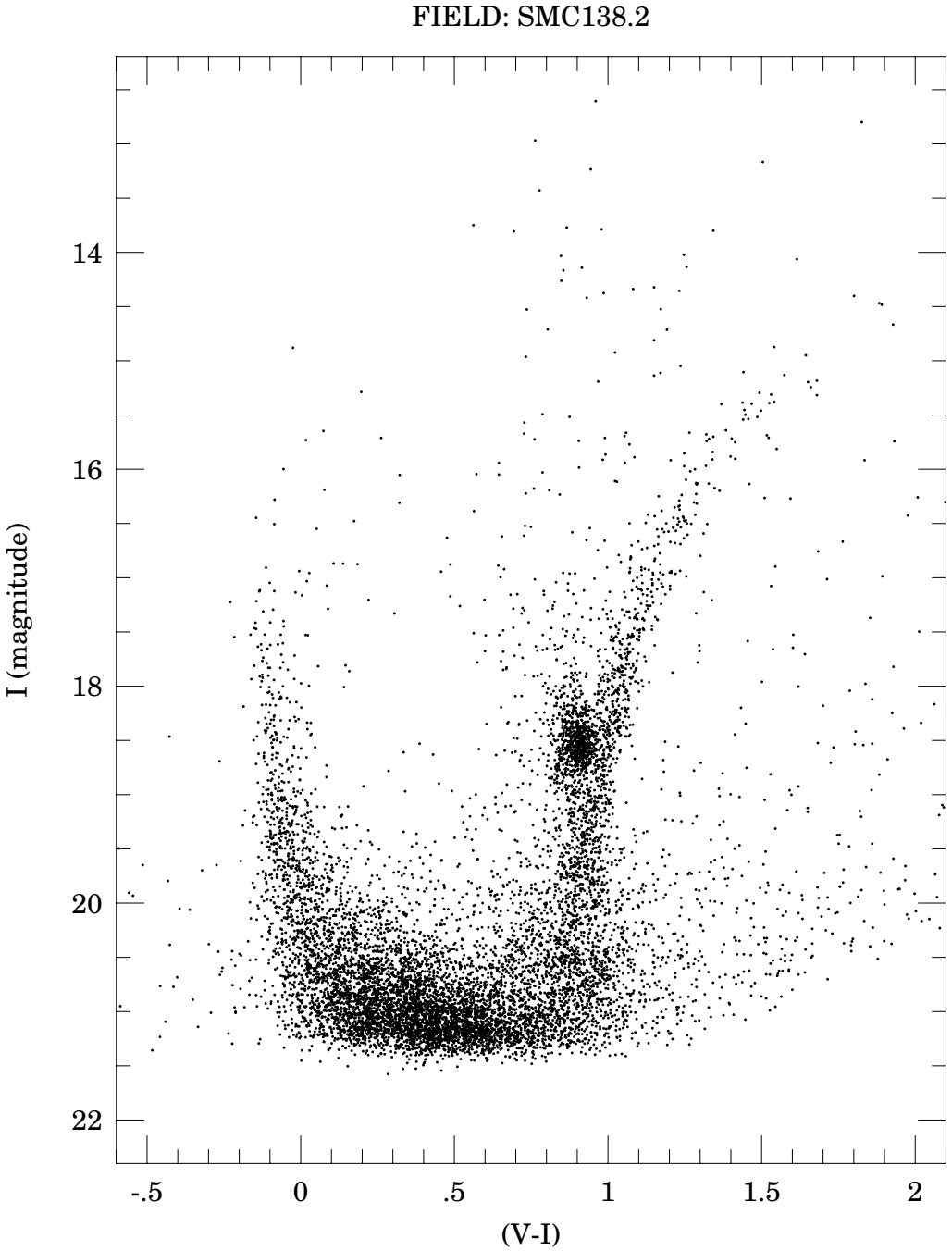

Fig. 8. Color–magnitude diagram of the western wing subfield SMC138.2

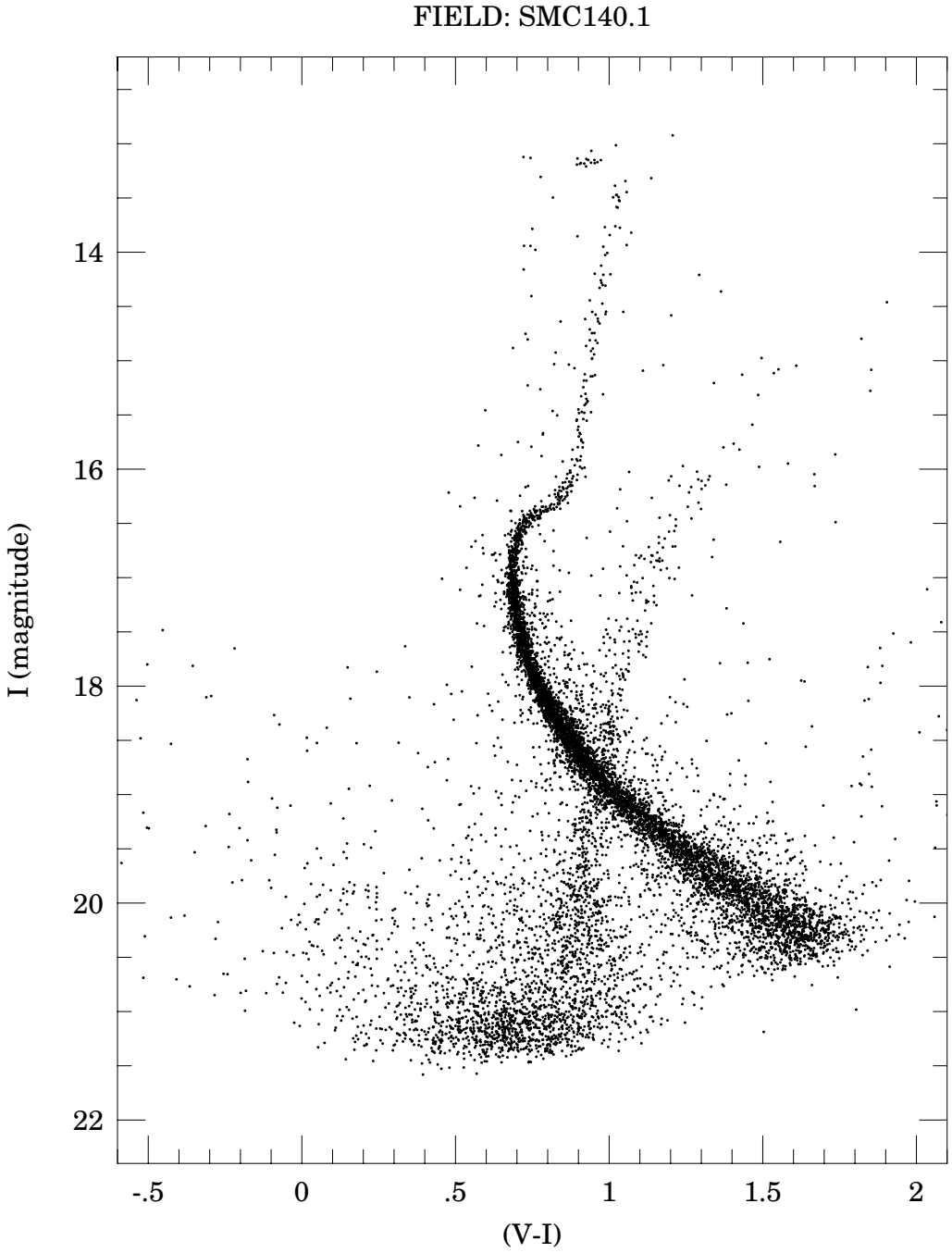

Fig. 9. Color–magnitude diagram of the field SMC140.1 covering outer parts of the 47 Tuc globular cluster.

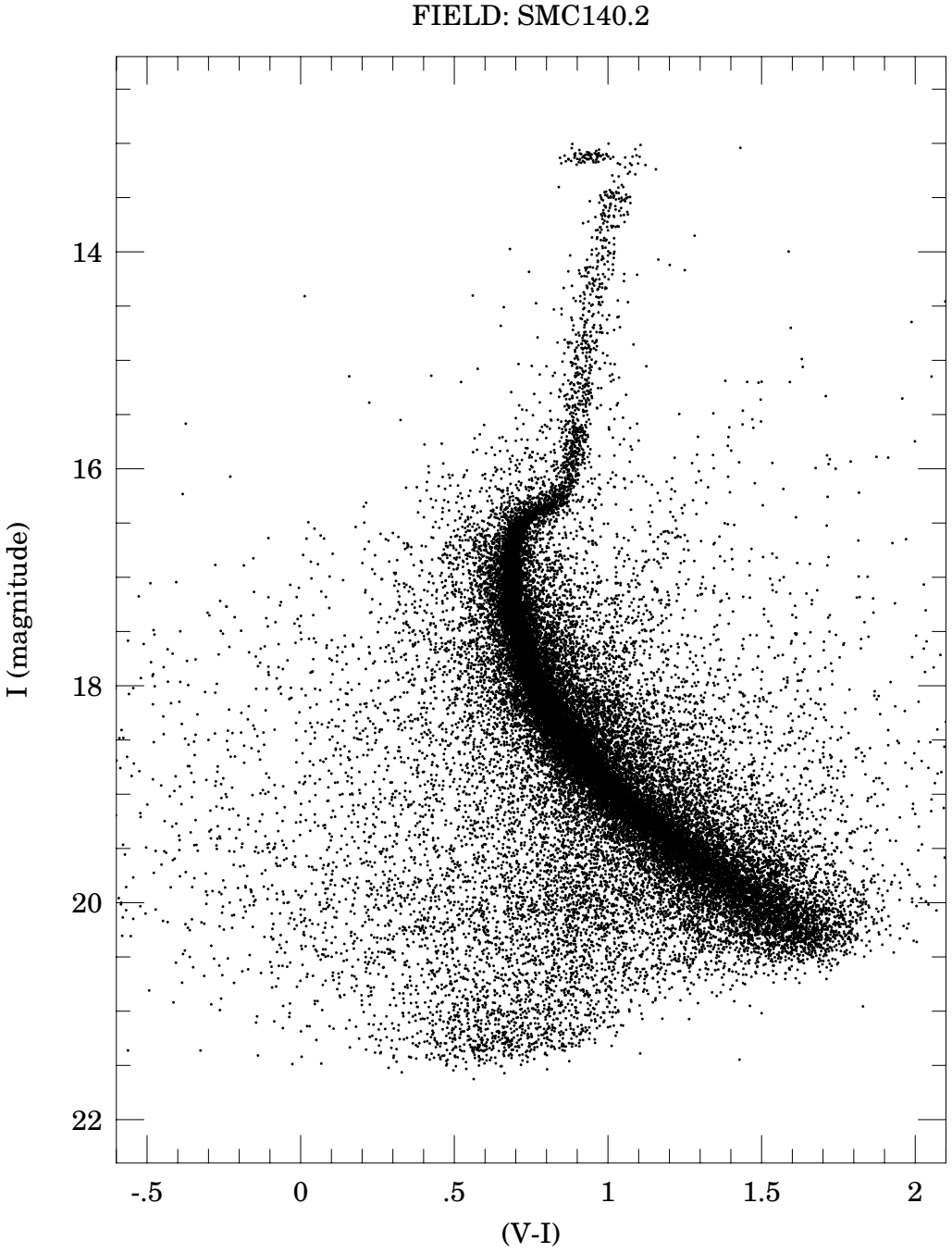

Fig. 10. Color–magnitude diagram of the field SMC140.2 covering part of the core of the 47 Tuc globular cluster.

Figs. 6–8 present, as an example of direct application of the OGLE-III maps, color–magnitude diagrams (CMDs) constructed for a few selected subfields from different parts of the SMC. They include the central bar field, as well as less dense regions of this galaxy from both sides of the bar. It is believed that the SMC has a considerable depth along the line of sight. This can indeed be easily noted comparing position of the red clump in the fields located on the opposite sides of the SMC bar (Figs. 7 and 8).

The SMC140 field is of particular interest. It was centered on the Galactic globular cluster 47 Tuc and covers practically the whole cluster. Fig. 9 presents spectacular CMD the outer regions of 47 Tuc (subfield SMC140.1) superimposed on the CMD of the SMC background stars while Fig. 10 – the CMD of the central parts of 47 Tuc (subfield SMC140.2). Very precise, unique and precisely calibrated photometry of 47 Tuc can be used for many scientific projects related to this cluster.

It should be noted, however, that the standard OGLE-III data pipeline is not optimized for the extremely dense central regions of the cluster with high stellar gradients. Therefore the presented photometry in the very central core regions of 47 Tuc is less complete than could be achieved with optimized procedures. We plan to rereduce the collected OGLE-III 47 Tuc images with the optimized software to obtain the photometry as complete as possible in the core of this cluster.

It is worth noting that OGLE-III maps also contain photometry of many other stellar clusters located in the SMC.

5. Data Availability

The OGLE-III Photometric Maps of the SMC are available to the astronomical community from the OGLE Internet Archive:

http://ogle.astrouw.edu.pl
ftp://ftp.astrouw.edu.pl/ogle3/maps/smc/

Beside tables with photometric data and astrometry for each of the subfields also the *I*-band reference images are included. Usage of the data is allowed under the proper acknowledgment to the OGLE project.

Acknowledgements. This paper was partially supported by the following Polish MNiSW grants: N20303032/4275 to AU and NN203293533 grant to IS and by the Foundation for Polish Science through the Homing (Powroty) Program.

REFERENCES

Chiosi, E., and Vallenari, A. 2007, *A&A*, **466**, 165.
Coe, M.J., Edge, W.R.T., Galache, J.L., and McBride, V.A. 2005, *MNRAS*, **356**, 502.
Evans, C.J., Howarth, I.D., Irwin, M.J., Burnley, A.W., and Harries, T.J. 2004, *MNRAS*, **353**, 601.

Haberl, F., Eger, P., and Pietsch, W. 2008, *A&A*, **489**, 327.
Pojmański, G. 1997, *Acta Astron.*, **47**, 467.
Udalski, A., Szymański, M., Kubiak, M., Pietrzyński, G., Woźniak, P., and Żebruń, K. 1998, *Acta Astron.*, **48**, 147.
Udalski, A., Szymański, M., Kubiak, M., Pietrzyński, G., Soszyński, I., Woźniak, P., and Żebruń, K. 2000, *Acta Astron.*, **50**, 307.
Udalski, A., Szymański, M., Kubiak, M., Pietrzyński, G., Soszyński, I., Woźniak, P., Żebruń, K., Szewczyk, O., and Wyrzykowski, Ł. 2002, *Acta Astron.*, **52**, 217.
Udalski, A. 2003, *Acta Astron.*, **53**, 291.
Udalski, A., Szymański, M.K., Soszyński, I., and Poleski. R. 2008a, *Acta Astron.*, **58**, 69.
Udalski, A., Soszyński, I., Szymański, M.K., Kubiak, M., Pietrzyński, G., Wyrzykowski, Ł., Szewczyk, O., Ulaczyk, K., and Poleski. R. 2008b, *Acta Astron.*, **58**, 89.